Random acoustic metamaterial with a subwavelength dipolar resonance

Mickaël Duranteau, Tony Valier-Brasier, Jean-Marc Conoir, Régis Wunenburger

▶ **To cite this version:**

Mickaël Duranteau, Tony Valier-Brasier, Jean-Marc Conoir, Régis Wunenburger. Random acoustic metamaterial with a subwavelength dipolar resonance. Journal of the Acoustical Society of America, 2016, 139 (6), pp.3341-3352. 10.1121/1.4950727 . hal-01344804

HAL Id: hal-01344804
https://hal.science/hal-01344804

Submitted on 12 Jul 2016

HAL is a multi-disciplinary open access archive for the deposit and dissemination of scientific research documents, whether they are published or not. The documents may come from teaching and research institutions in France or abroad, or from public or private research centers.

L'archive ouverte pluridisciplinaire **HAL**, est destinée au dépôt et à la diffusion de documents scientifiques de niveau recherche, publiés ou non, émanant des établissements d'enseignement et de recherche français ou étrangers, des laboratoires publics ou privés.

Distributed under a Creative Commons Attribution - ShareAlike 4.0 International License

Random acoustic metamaterial with a subwavelength dipolar resonance

Mickaël Duranteau,[1] Tony Valier-Brasier,[1,a)] Jean-Marc Conoir,[1] and Régis Wunenburger[2,b)]
[1]*Sorbonne Universités, UPMC Univ Paris 06, CNRS, UMR 7190, Institut Jean Le Rond d'Alembert (∂'Alembert), 4, Place Jussieu, F 75005, Paris, France*
[2]*Université de Bordeaux, CNRS, UMR 5798, Laboratoire Ondes et Matière d'Aquitaine (LOMA), 351 Cours de la Libration, F 33400 Talence, France*

The effective velocity and attenuation of longitudinal waves through random dispersions of rigid, tungsten-carbide beads in an elastic matrix made of epoxy resin in the range of beads volume fraction 2% 10% are determined experimentally. The multiple scattering model proposed by Luppé, Conoir, and Norris [J. Acoust. Soc. Am. **131**(2), 1113 1120 (2012)], which fully takes into account the elastic nature of the matrix and the associated mode conversions, accurately describes the measurements. Theoretical calculations show that the rigid particles display a local, dipolar resonance which shares several features with Minnaert resonance of bubbly liquids and with the dipolar resonance of core-shell particles. Moreover, for the samples under study, the main cause of smoothing of the dipolar resonance of the scatterers and the associated variations of the effective mass density of the dispersions is elastic relaxation, i.e., the finite time required for the shear stresses associated to the translational motion of the scatterers to propagate through the matrix. It is shown that its influence is governed solely by the value of the particle to matrix mass density contrast.

I. INTRODUCTION

As proposed from the very beginning of research on acoustic metamaterials,[1] a successful strategy for obtaining negative effective density, compressibility, or refractive index is to exploit the intrinsic (so-called local) resonances of mechanical resonators having a subwavelength size and embedded in the propagation medium. Compared to the phononic crystals strategy, the strategy based on local resonances benefits from mainly two advantages. First, the targeted properties can *a priori* be obtained without any crystalline order of the embedded resonators, although order may play a significant role. Second, since at resonance the acoustic wavelength in the embedding medium can be large compared to the resonator size, depending on the resonator design and performances, the targeted properties can be obtained using extremely thin samples compared to wavelength. Reported efficient locally resonant metamaterials (LRM) involve mechanical resonators with various degrees of sophistication and assembled in one, two, or three dimensions: Helmholtz resonators,[2–4] air bubbles in liquids,[5] solid membranes, either loaded[6] or unloaded,[7] liquid films in foams,[8] core-shell particles,[1] mass-spring systems,[9] "slow" spheres,[10] rod-spring resonators,[11] hollow tubes,[12] and various combinations of them.[11,13,14] In the audible domain several applications of LRM have already been implemented, which involve handmade or machined, resonators with centimeter size. In the ultrasonic domain, several applications of LRM are also foreseen. Their practical implementation raises several issues such as the resonators miniaturization and assembly,[15] or the detailed knowledge of elastic properties of the materials constituting the resonators at ultrasonic frequencies.[16]

We focus on the dense core-soft shell particles, which have been used in the first LRM[1] and have been extensively studied theoretically. This kind of resonator can be sketched as a mass-spring resonator where the oscillating mass is the rigid, dense core and the spring is the compliant shell deformed by the core displacement.[17,18] The high density of the core ensures that the phase delay of the core motion with respect to the matrix motion above the resonance frequency has a noticeable impact on the effective density of the LRM.[17,19] The softness of the shell results in a small resonance frequency, ensuring that the wavelength in the embedding medium is large compared to the resonator size. Although this kind of resonator has allowed to obtain negative effective density in the audible domain,[1] its complex structure and the large dissipation in the viscoelastic shell at ultrasonic frequencies, which dampens the resonance,[19] makes them difficult to implement in the ultrasonic domain. As shown by Kinra *et al*. in the 1980s,[20,21] another kind of composite material actually displays a solid body translation resonance, i.e., a similar local resonance, namely, a dispersion of dense, hard particles in a less dense, elastic matrix. Given the prolific worldwide research on metamaterials, it is surprising that such a simple kind of LRM has, to our knowledge, never been studied by the metamaterials community,

[a)]Electronic mail: tony.valier brasier@upmc.fr
[b)]Current address: Sorbonne Universités, UPMC Univ Paris 06, CNRS, UMR 7190, Institut Jean Le Rond d'Alembert (∂'Alembert), 4, Place Jussieu, F 75005, Paris, France.

in particular, regarding its effective properties around its local resonance. More generally, as pointed in one of the last reviews on this kind of material,[22] there is a lack of experimental data on the acoustic properties of dispersions of dense, rigid particles. In this article, we provide original, comprehensive, and accurate data on effective acoustic properties of random dispersions of dense, tungsten-carbide (TC) beads in an epoxy matrix around their local resonance frequency in the 0.1 2.5 MHz frequency range. From a theoretical point of view, while acoustic propagation in such dispersions at frequencies smaller than the local resonance frequency has been the subject of several works,[22] the influence of the local resonance on acoustic propagation has actually been much less studied.[36] In this article, we compare over the entire investigated frequency range our experimental data with several multiple scattering theories, in particular, with a recent model[42] which takes into account the effect of longitudinal-transverse wave conversions on the scattering of waves.

Our article is organized as follows. In Sec. II, we present the acoustic properties of the beads and matrix and we detail the samples fabrication protocol. Then, we describe the acoustic measurements and signal analysis procedures. In Sec. III, we briefly present the ingredients of the multiple scattering theories, which we aim to confront to our measurements, and we thoroughly compare our experimental data to these theories. Finally, in Sec. IV, we provide several physical insights in the scatterer dynamics and in the acoustic propagation in these dispersions. We evidence the strong similarities of this kind of resonance with Minnaert's resonance in bubbly liquids. We identify the causes of smoothing of the dipolar resonance and evaluate their impact on the behavior of the effective mass density of the dispersions.

II. EXPERIMENTS

A. Materials properties

The composite material under study is a suspension of dense, TC spherical particles (labeled by p in the following) with monodisperse diameter, randomly dispersed in a matrix made of epoxy resin.

We used spherical, submillimetric TC beads supplied by Marteau-Lemarié (Pantin, France) and having nominal density $\rho_p = 14.95 \times 10^3$ kg m ^{3} and Lamé constants $\lambda_p = 2.09 \times 10^{11}$ Pa and $\mu_p = 2.66 \times 10^{11}$ Pa. Two bead sizes have been used, 397 μm and 500 μm nominal diameter $2R$, with small nominal diameter dispersity (± 2.5 μm).

Epoxy resin, "2-Ton" model supplied by ITW Devcon (Danver, MA), has nominal density $\rho = 1100$ kg m ^{3}. It has been chosen for its rather long curing time (30 min), which allows for (i) a quiet insertion of the beads, (ii) a reasonable heat release rate during curing, and (iii) time for enclosed air bubbles to rise and burst.

Even once cured, epoxy is well known to display a pronounced viscoelastic behavior in the ultrasonic frequency domain, as a consequence of its polymeric nature. In order to access the epoxy viscoelastic properties, frequency-dependent velocities and attenuations of both longitudinal (compression) and transverse (shear) waves in cured epoxy have been measured. The velocity c_L and attenuation α_L of longitudinal waves in epoxy have been determined from transmission measurements pulses with 2.25 MHz central frequency at normal incidence through a 9.43 mm thick epoxy slab immersed in water using the same protocol as for the beads dispersion samples described below. The velocity c_T and attenuation α_T of transverse waves in epoxy have been determined from transmission measurements of longitudinal pulses with 2.25 MHz central frequency through slab immersed in water and inclined with an incidence angle ($\theta = 55°$) larger than the first critical angle of water epoxy interface in order to suppress the transmission of longitudinal waves through the slab and to exploit the longitudinal-transverse-longitudinal wave conversion at water epoxy interfaces, according to the method described in Ref. 23. The measured variations of the velocities and attenuations of both longitudinal and transverse waves in epoxy as a function of frequency are plotted in Figs. 1(a) and 1(b), respectively.

The complex Lamé constants λ and μ of epoxy are then determined from the relationships $c_L = \sqrt{(\lambda + 2\mu)/\rho}$ and $c_T = \sqrt{\mu/\rho}$. The frequency-dependence of the Lamé

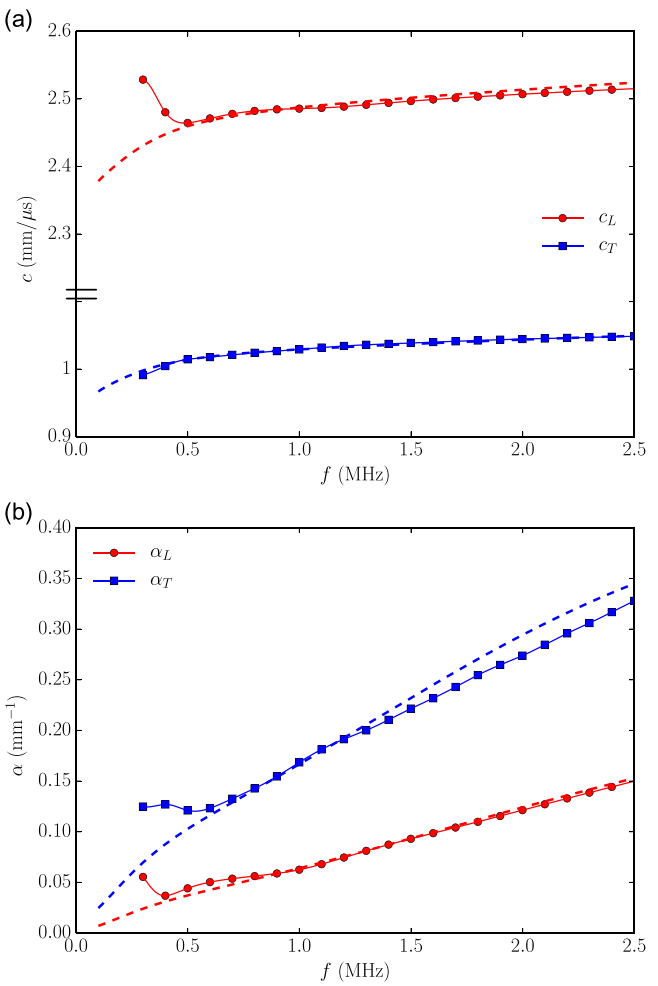

FIG. 1. (Color online) (a) Experimental variations of the longitudinal velocity c_L (curve decorated with full circles) and the transverse velocity c_T (curve decorated with full squares) as functions of the frequency in epoxy resin. Dashed curves are best fits to the measurements based on Eq. (1). Experimental frequency resolution is 5 kHz. (b) Same for attenuations α_L and α_T.

TABLE I. Best fit values [based on Eq. (1)] of the parameters defining Lamé coefficients of epoxy resin.

	λ	μ
C_0 ($\times 10^9$ Pa)	3.6	1.05
C_1 ($\times 10^9$ Pa)	0.1	0.2
τ_1 ($\times 10^{-9}$ s)	5000	5000
C_2 ($\times 10^9$ Pa)	0.3	0.15
τ_2 ($\times 10^{-9}$ s)	500	500
C_3 ($\times 10^9$ Pa)	0.25	0.1
τ_3 ($\times 10^{-9}$ s)	50	14
C_4 ($\times 10^9$ Pa)	0.3	0.15
τ_4 ($\times 10^{-9}$ s)	8	50

constants, which result from the relaxation of the polymers, can be accurately described using the classical Zener model of viscoelastic materials.[24,25] As shown in Figs. 1(a) and 1(b), satisfactory fits to the experimental data could be obtained using only four relaxation times τ_n, $n = 1\ 4$, which are related to the Lamé constants according to the following expressions:[26]

$$C(\omega) = C_0 + \sum_{n=1}^{4} C_n \frac{(\omega\tau_n)^2 - i\omega\tau_n}{1 + (\omega\tau_n)^2}, \quad (1)$$

where C stands for λ or μ, C_0 is its low frequency value, and C_n, $n = 1\ 4$ are weighting coefficients associated to relaxation times τ_n. The values of the relaxation times and associated coefficients corresponding to these best fits are given in Table I. Noticeably, the values of relaxation times are in good agreement with values reported in Ref. 24. For accuracy and simplicity purposes, these analytical approximations of the Lamé constants of epoxy are used in the following instead of their measured values.

B. Samples preparation

Despite the large viscosity of uncured epoxy, the beads density is so large that sedimentation occurs during the curing, even with more rapidly curing resins. Consequently, three-dimensional, homogeneous samples could not be obtained by simply stirring the epoxy-beads mixture before solidification. Thus, beads dispersions having volume fractions ranging from $\phi = 2\%\ 10\%$ were manufactured layer by layer according to the following protocol.

The lengthy spreading of the viscous resin poured at each step, competing with its solidification and the impossibility to steer the resin without enclosing bubbles, imposed a minimum resin height of 1 mm for each layer for a full and homogeneous coverage of the sample surface.

Cylindrical, 55 mm diameter Petri dishes were chosen as molds. Once the sample thickness e and the beads volume fraction ϕ had been chosen, the corresponding mass of beads was weighted and the beads set was split into N subsets, $N = e - 1$ (with e expressed in millimeters) being the number of layers which are expected to constitute the sample. In a horizontal Petri dish previously covered with a mold release wax (reference 66 333MR-1000P from Finish Care Products, South El Monte, CA), a reproducibly $h = 1$ mm thick layer of resin was poured. A subset of beads was randomly dispersed 20 min after, and then curing was achieved in 10 min. This sequence was repeated N times. Finally, a layer of epoxy was poured and cured, which allowed the sample top surface to be planar, and then the sample was removed from its mold. h is smaller than the average distance between nearest neighbors in a random dispersion which is expressed as $0.9R\phi^{-1/3}$ (Ref. 27) and varies from 650 μm (respectively, 820 μm) to 300 μm (respectively, 380 μm) for 397 μm (respectively, 500 μm) diameter beads in the investigated range of volume fractions. Consequently, the resulting beads distribution displays some anisotropy, whose importance increases with volume fraction. Noticeably, h is smaller than the smallest wavelength in resin $\lambda_{\min} = 1$ mm, met for $f = 2.5$ MHz, which allows us to ignore phononic effects. The characteristic features of all the samples produced for this study are given in Table II.

C. Acoustic measurements

The acoustic properties of the samples were determined by performing underwater longitudinal wave transmission measurements at normal incidence. The samples, fixed on a tapped panel having an air gap inside, were immersed in a water tank. Three pairs of Olympus (Tokyo, Japan) identical piezoelectric transducers having different central frequencies f_t and diameters (see Table III) were used, which allowed us to reliably cover the frequency range $[0.1, 2.5]$ MHz. The sample was placed in the far field of the emitter [distance slightly larger than $(D/2)^2 f/c_0$, where D is the transducer diameter and c_0 the sound velocity in water] in order to be probed with plane waves; see Table III.[28] The receiver was facing the emitter and located close to the sample (i.e., 20 mm away) in order to avoid possible diffraction effects by the sample-screen junction.[29,30]

The emitting transducer was fed with a standard pulser-receiver (reference 5072 from Olympus). The transmitted signal detected by the receiving transducer was acquired at a 5×10^9 samples per second sampling rate and averaged over 1024 acquisitions using a digital oscilloscope (this resulted in a frequency resolution of 5 kHz of the Fourier transform of the signals). Figure 2 displays two sets of 1 MHz and 2.25 MHz central frequency (f_t) signals transmitted through water and a 8.82 mm thick slab of a dispersion of 397 μm beads with volume fraction $\phi = 5\%$. Comparing the signals received after propagation through the beads dispersion (signal S in Fig. 2) to the signals received after propagation through water (signal S_0) and anticipating the spectral signal analysis, one can state that: (i) the earlier arrival of the signal is due to the larger velocity of longitudinal waves, (ii) the signal lengthening is due to the strong dispersion, (iii) the apparent change in central frequency of the 1 MHz signal results from the large attenuation for frequencies larger than 0.5 MHz.

As the acoustic pulse propagates through the suspension, it is scattered by the beads. The resulting wave propagating through a sample can be described as the superposition of a coherent wave independent of the beads distribution and an incoherent wave which depends on the beads distribution. The contribution of the incoherent wave to the received signal

TABLE II. Characteristic features of the samples used for this study. The standard deviation of the sample thickness, computed from a series of random thickness measurements throughout the entire sample surface, characterizes the flatness of the sample and the parallelism of its faces.

Beads volume fraction ϕ (%)	Beads diameter $2R$ (μm)	Sample thickness $e \pm$ standard deviation (mm)
0		9.43 ± 0.01
2	397	5.51 ± 0.04
	397	8.48 ± 0.01
	397	19.17 ± 0.04
	500	4.87 ± 0.04
5	397	5.10 ± 0.09
	397	8.82 ± 0.02
	397	19.16 ± 0.04
	500	5.15 ± 0.09
7.5	500	3.23 ± 0.12
10	397	3.36 ± 0.06
	500	5.68 ± 0.03

depends on the pulse central frequency, which determines the efficiency of the scattering, on the sample thickness and acoustic beam diameter, which both determine the number of irradiated scatterers, but also on the receiver diameter since the spatial fluctuations of the incoherent wave in the receiver plane are averaged over the receiver surface. In order to reduce the contribution of the incoherent wave to the received signal, the latter is also averaged over 16 acquisitions performed at 16 different sample positions corresponding to the nodes of a 4×4, 2 mm step squared grid lying in the sample plane. By doing this, an averaging over the scatterers distribution is performed. The contribution of the incoherent wave to the signals can be evaluated by comparing a signal acquired at a particular grid node (signal S) and the averaged signal (signal S_a), both shown in Fig. 2. While this contribution is barely visible at $f_t = 1$ MHz, it is more pronounced at $f_t = 2.25$ MHz. This may be explained as the result of both larger wave scattering at higher frequency and the smaller diameter of the $f_t = 2.25$ MHz receiver compared to the one of the $f_t = 1$ MHz receiver (see Table III). However, there is no pronounced delayed signal resulting from multiple scattering. These observations justify our spatial averaging process for isolating the contribution of coherent wave in the transmitted signal.

D. Signal analysis

The longitudinal wave transmission coefficients of the samples were determined as function of frequency from the comparison between the averaged signal $S_a(t)$ (t is time) transmitted through the beads dispersion sample and the signal $S_0(t)$ transmitted through water, i.e., in absence of sample, according to the following procedure.

TABLE III. Characteristic features of the transducers used for the experiments and associated working conditions.

Olympus reference	V301	V302	V323
Diameter (inch)	1	1	0.25
Central frequency f_t (MHz)	0.5	1	2.25
Exploitable frequency range (MHz)	0.1 0.6	0.1 1.2	0.3 2.5
Emitter sample distance (mm)	70	120	40

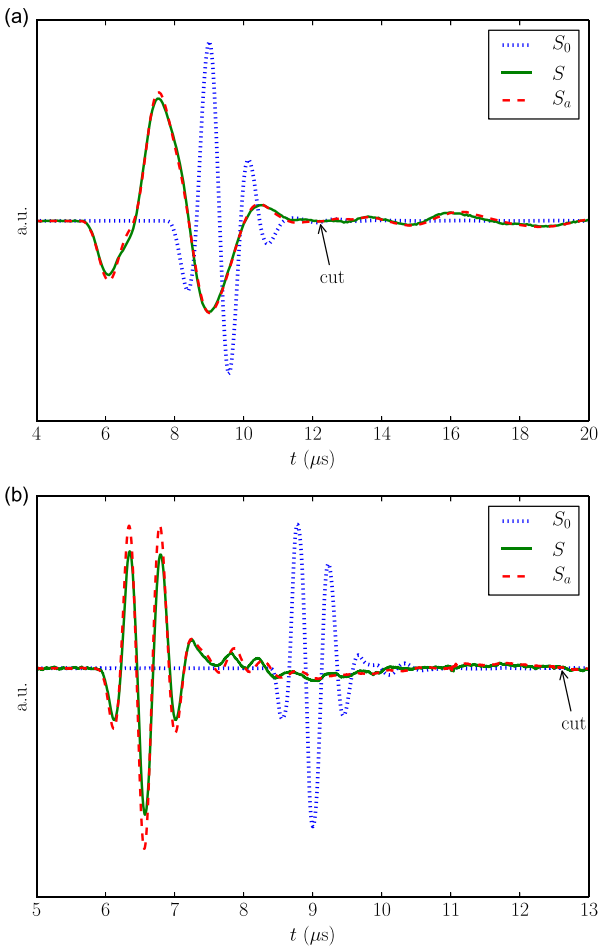

FIG. 2. (Color online) Typical acoustic signals with central frequency (a) f_t 1 MHz and (b) f_t 2.25 MHz transmitted through water (dotted curve, signal labeled S_0) and through a e 8.82 mm thick sample filled with volume fraction ϕ 5% of 397 μm beads (solid curve, signal labeled S acquired along a given path through the sample; dashed curve, signal labeled S_a averaged over 16 different paths through the sample). The signals transmitted through the sample have been multiplied by a factor of 10 and 35 in (a) and (b), respectively.

In order to isolate the signal having propagated through the sample only once, only the part of S_a beginning just before the main peak and lasting $2e/c_{\max}$ was retained, the other part of S_a begin padded with zeroes. $c_{\max} = 2600$ m s^{-1} is the maximum velocity measured in the samples (see below). More precisely, the end of the rectangular window applied to S_a was slightly tuned to coincide with a zero of S_a in order to avoid any signal discontinuity. The same filter was applied to S_0. Then, the Fourier transforms of S_a, $\hat{S}_a(f)$ and S_0, $\hat{S}_0(f)$, were computed using *Python* language. With the aim of accurately unwrapping the phase of $\hat{S}_a/\hat{S}_0$ later, $\hat{S}_a$ (respectively, $\hat{S}_0$) was multiplied by $\exp[-i\omega t_p^1]$ (respectively, $\exp[-i\omega t_p^0]$), where $\omega = 2\pi f$ is the angular frequency and t_p^1 (respectively, t_p^0) is the instant of detection of the main peak of S_a (respectively, S_0).[31] Finally, the real k' and imaginary k'' parts of the complex acoustic wavenumber k_L^{eff} in the sample were determined independently as functions of the frequency by fitting separately the modulus and the phase of the complex transmission factor $T_1 T_2 \exp[i(k_L^{\text{eff}} - k_0)e] \exp[i\omega(t_p^1 - t_p^0)]$ to the ratio

$\hat{S}_a/\hat{S}_0$, where $k_0 = \omega/c_0$ is the real, acoustic wavenumber in water, c_0 is the sound velocity in water computed from temperature measurement in the tank,[32] $\rho_0 = 1000$ kg m ^{3} is the density of water at room temperature, and $T_1 = 2Z_L/(Z_0 + Z_L)$ and $T_2 = 2Z_0/(Z_0 + Z_L)$ are the pressure transmission coefficients of water-epoxy and epoxy water interfaces, respectively, with $Z_i = \rho_i c_i$, $i = 0, L$. This allowed us to calculate the velocity $c_L^{\text{eff}} = \omega/k'$ and the attenuation $\alpha_L^{\text{eff}} = k''$ of longitudinal waves in the sample.[33,34] We are aware that Z_L should be ideally computed using the effective impedance of the composite material and not of epoxy. Since this effective impedance is actually unknown, this leads to a complicated implicit problem. This is the reason why we adopted this approximate definition for Z_L.

Since the pulse duration has to be shorter than the round-trip time in the sample, thin samples are obviously not adapted to low frequency measurements. Conversely, since strong attenuation occurs at frequencies larger than 0.5 MHz, thick samples are not adapted to high frequency measurements because acoustic transmission through them is too much attenuated. Consequently, when samples with several different thicknesses were available, among all the measurements on the thinnest sample only those corresponding to $f_t = 0.5$ MHz were retained, while among all the measurements on the thickest sample, only those corresponding to $f_t = 1$ MHz and 2.25 MHz were retained. This selection based on physical considerations was found to ensure in practice good consistency between all the selected measurements all over the investigated frequency range.

III. COMPARISON BETWEEN EXPERIMENT AND THEORY

A. Theory

It is commonly assumed that the multiple scattering of an acoustic wave by a random distribution of scatterers may be described as resulting in a coherent wave being the acoustic field averaged over all possible scatterer configurations. The propagation of this coherent wave is characterized by a complex-valued, effective wavenumber, whose imaginary part accounts for the energy loss due to scattering in all directions. The multiple scattering of waves in media through only one kind of wave can propagate, like fluid media, has been the object of numerous models in the last decades. Reviews of these models and their mathematical backgrounds can be found in Refs. 37 39. By contrast, the multiple scattering of waves in media where several kinds of waves can propagate and wave conversion can occur, like elastic media through which both compression (L) and shear waves (T) can propagate, has been the object of much fewer models (see Refs. 40 42, and references therein). From a mechanical point of view, the contribution of wave conversion to the coherent wave originates from the fact that a scatterer put into motion by an L wave scatters not only an L wave but also a T wave. When this T wave attains its neighbors, it puts them into motion. They emit, in turn, L waves, which contribute to the effective L wave. This explains why the influence of wave conversion on the coherent wave vanishes (i) in the $\phi \to 0$ limit, i.e., when neighboring scatterers are distant, and (ii) in the case of strong T dissipation in the matrix, i.e., when shear waves are strongly attenuated along their path from a scatterer to another.

For the case of randomly distributed elastic spheres in elastic media, explicit models, in which effective wavenumber is given by an explicit formula,[42] and self-consistent models, in which it is the solution of a characteristic equation,[40] have been proposed. In the following, the explicit model derived in Ref. 42 is preferred because it allows to clearly identify the contributions of wave conversions ("coupling terms"). More precisely, the effective wavenumbers of coherent L and T waves are derived in the spirit of Fikioris and Waterman's approach,[43] which is based on the quasi-crystalline assumption and takes account of the nonoverlap between the scatterers ("hole correction"). In this model, the parameter b (hole radius) introduced in the course of the field averaging process satisfies $b = 2R$. In the following, the effective wavenumber of the coherent compression wave predicted using this model is labeled LCN model. Interestingly, direct numerical simulations of multiple scattering in concrete[44] have confirmed the validity of LCN model in the case of weak scattering up to densities of 25%.

Note that, in the long wavelength limit, LCN ($b \to 0$) model identifies with Linton and Martin's model[37] (hereafter, labeled LM model) with an additional contribution due to wave conversion. This remark will later lead us to conclude on the influence of wave conversion on coherent propagation from the benchmarking of LCN and LM models against experiments.

B. Experimental results

We now confront the above presented theoretical predictions to the measurements. Figures 3, 4, and 5 display the experimental variations of the velocity and attenuation of longitudinal coherent waves together with their predictions using LM and LCN models as functions of f and $k_L^0 R$ ($k_L^0 = \omega/c_L^0$, c_L^0 being the zero-frequency value of the longitudinal velocity in epoxy $c_L^0 = 2276.4$ m s ^{1}) in dispersions of 397 μm diameter beads in epoxy with volume fractions $\phi = 2\%$, 5%, and 10%, respectively. The discrepancy between the superposed experimental curves obtained using different transducers (see above) can be regarded as an evaluation of the overall uncertainty associated to the measurements.

As a preamble, we note that strong dispersion and attenuation, which are the signature of a resonance, occur around $k_L^0 R \simeq 0.3$. This demonstrates that this resonance is actually subwavelength. First, LCN model is observed to fit to the experimental data globally much better than LM model for all volume fractions. In particular, the velocity peak predicted by LM model (and not by LCN model) is not reproduced by the experimental data. This definitely demonstrates that wave conversions play a key role in the propagation of coherent waves in elastic media and that LCN model fairly describes the influence of wave conversion. Second, for $\phi = 5\%$ and 10%, LCN model is observed to fit to the experimental attenuation better than LCN ($b \to 0$) model. This confirms the relevance of the hole correction in LCN model.

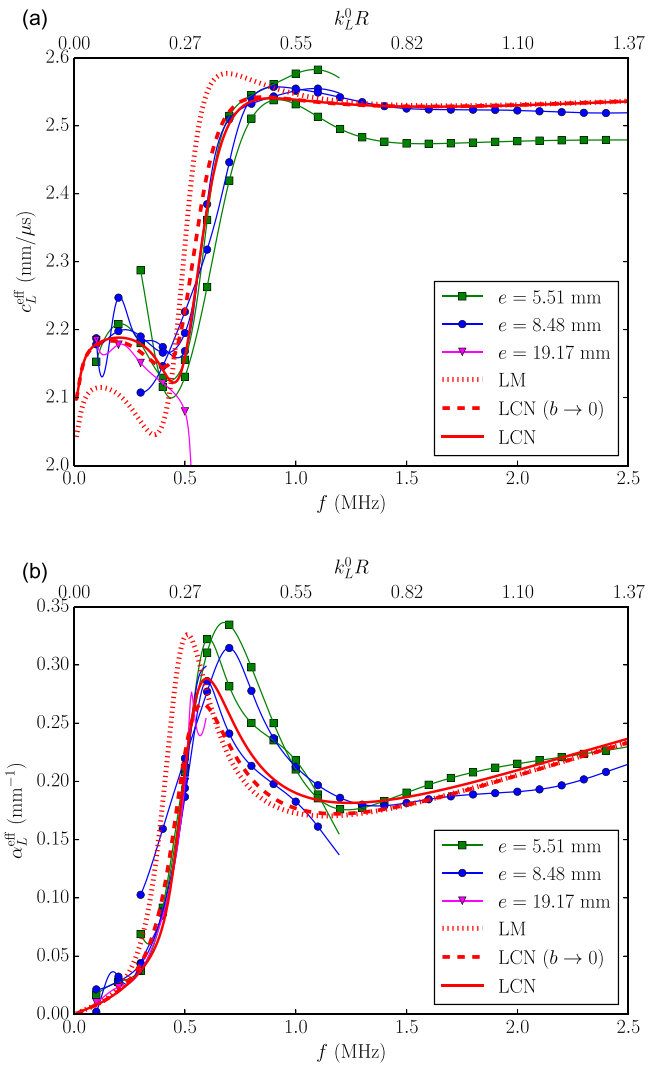

FIG. 3. (Color online) Variations of (a) velocity $c_L^{\rm eff}$ and (b) attenuation $\alpha_L^{\rm eff}$ of the coherent longitudinal wave propagating through dispersions of 397 μm diameter beads in epoxy with volume fraction ϕ 2% as functions of frequency f and dimensionless wavenumber $k_L^0 R$. Solid curves decorated with symbols, experimental data with 5 kHz frequency resolution obtained using various samples and transducers (see inset legend and Tables II and III); bold curves, theoretical predictions using LM model (dotted curve), LCN ($b \to 0$) model (dashed curve), LCN model (solid curve).

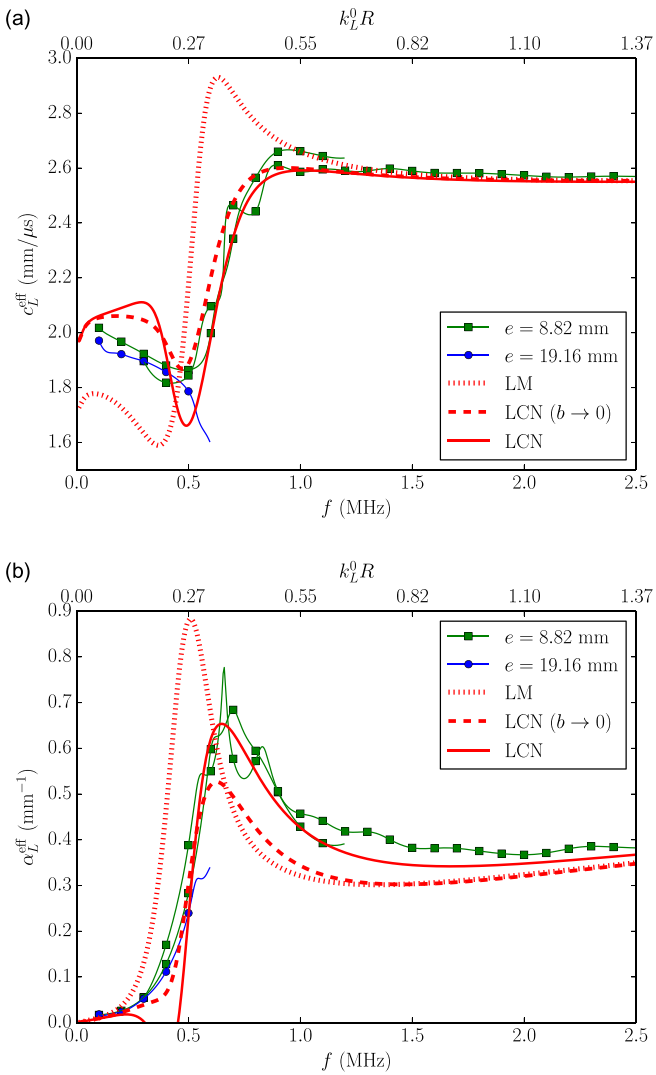

FIG. 4. (Color online) Same as Fig. 3 for ϕ 5%.

The agreement between LCN model and experimental data is found to be excellent for $\phi = 2\%$ and for 5% for frequencies larger than 0.5 MHz. This demonstrates the accuracy of LCN model. Conversely, the discrepancy between LCN model and the experimental data for $\phi = 10\%$ is quite large. This can be attributed to the loss of accuracy of analytical models at high volume fractions in the case of strong scattering due to the sphere resonance. The discrepancy between theory and experiment observed in this frequency range could also be due to the anisotropy of the samples, which could blur this fine behavior. Noticeably, LCN model displays negative attenuation and simultaneously positive velocity around 0.4 MHz for $\phi = 5\%$ and 10%, whereas the experimental velocity and attenuation are both positive in this frequency range. This unphysical attenuation has already been observed by different authors[38,44,45] without explanation.

IV. FURTHER THEORETICAL DEVELOPMENTS

As pointed out by Moon and Mow,[36] the physical phenomenon responsible for the strong acoustic dispersion and attenuation observed around 0.5 MHz in elastic dispersions is the resonance corresponding to the particle deformation eigenmode labeled $n = 1$, also called the dipolar resonance of the scatterers. This allows us to call this resonance a *local resonance*, in contrast to spatial interferences involving inter-particle distance, like in phononic crystals.

The physical ground of dipolar scattering is the following. When the density (inertia) of the particles differs from that of the surrounding elastic matrix, the cyclic variations of the mechanical stress associated with the wave lead to oscillating motions of the matrix and of the particles having different amplitudes,[46] thus, on an oscillating relative motion of the particle with respect to the matrix. It follows that the particle scatters acoustic energy according to a dipolar pattern (associated to the dipolar resonance $n = 1$) if the particle is small with respect to the incident wavelength. The resonant behavior of the scatterer motion and the associated acoustic scattering relies on the combination of the particle

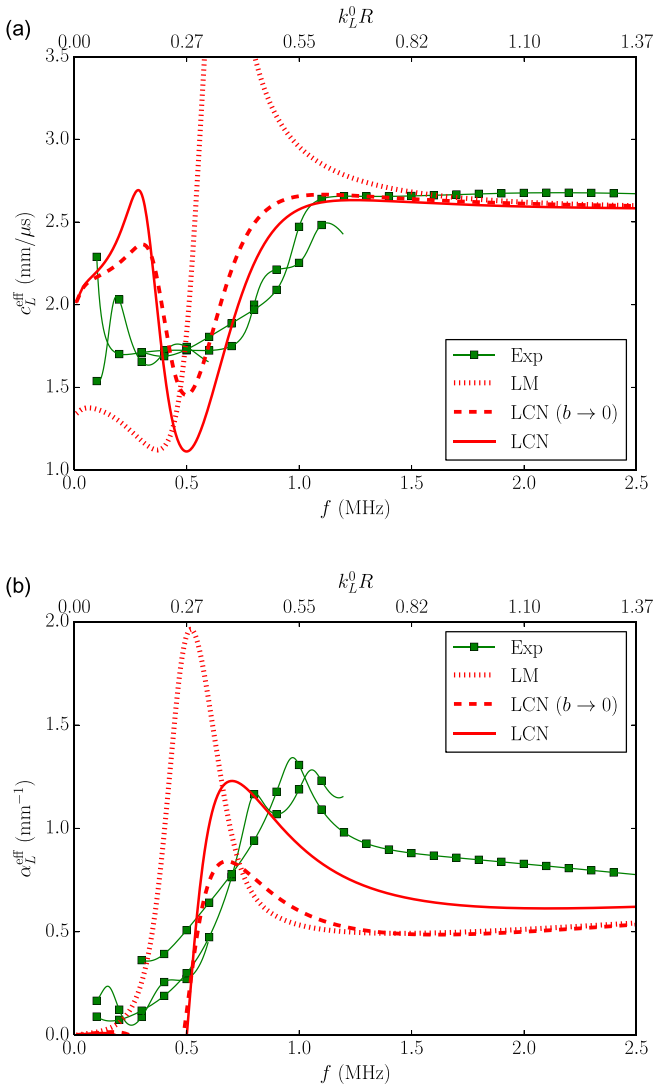

FIG. 5. (Color online) Same as Fig. 3 for ϕ 10%.

inertia and the elastic force exerted by the deformed matrix on the oscillating particle.

Although numerous studies have addressed the scattering of elastic waves by a solid inclusion,[47,48] only the pioneering work of Moon and Mow[36] deals with the effect of the dipolar resonance of the inclusion on the multiple scattering of sound. More precisely, in the latter study, the particle was assumed to be rigid and to undergo only solid body translation along the direction of propagation of the incident wave. For this reason, knowledge on the influence of the elastic properties of the particle on its resonance is lacking. Given this context, in this section physical interpretations of LCN model based on analytical calculations and parametric numerical studies are presented in order to gain a qualitative insight in this little-known resonance.

A. Resonance frequency in the limit of infinitely rigid scatterers

In a recently published work,[49] it has been shown that in the long wavelength regime, in the limit of large values of the shear modulus ratio $\tilde{\mu} = \mu_p/\mu$, the elastic properties of the scatterer excited by an incident longitudinal wave have a minor influence on the amplitudes of the modes $n = 1$ of the longitudinal and transverse scattered waves in the matrix contrary to its mass. Given the large contrast in elastic properties between TC and epoxy resin ($\tilde{\mu} \approx \mu_p/\mu_0 = 253$), it is thus reasonable to consider the scatterer as a moving rigid particle. In this limit, its dipolar vibration mode can be seen as a simple oscillatory translation, which is exactly the motion exploited in core-shell particles based LRM.

LCN model involves the scattering coefficients T_n^{LL} that describe the scattering of a longitudinal plane wave by a unique particle in the form of a longitudinal wave, as well as T_n^{LT} (respectively, T_n^{TL}) that describes the scattering of a longitudinal (respectively, transverse) plane wave in the form of a transverse (respectively, longitudinal) wave, i.e., the scattering coefficient associated to mode conversion $L \to T$ (respectively, $T \to L$). The effective wavenumber k_L^{eff} depends on these scattering coefficients as follows:

$$\left(\frac{k_L^{\text{eff}}}{k_L}\right)^2 = 1 - i\frac{3\phi}{(k_L R)^3}\sum_{n=0}^{\infty}(2n+1)T_n^{LL} + \phi^2 F\left(T_n^{LL}, T_n^{LT}, T_n^{TL}\right), \tag{2}$$

where the function $F(T_n^{LL}, T_n^{LT}, T_n^{TL})$ is given in Ref. 42. Accordingly, $L \to T$ and $T \to L$ mode conversions do not come up at first order in ϕ. This result is predicted by all the existing multiple scattering models.

We now aim to determine the eigenfrequency associated to the vibration eigenmode $n = 1$. Since at the dipolar resonance $|k_L R| < 1$, we consider for simplicity purpose the approximate expression of the dipolar scattering coefficient T_1^{LL} in the long wavelength regime $|k_L R| \ll 1$ (Ref. 49),

$$T_1^{LL} = \frac{i(k_L R)^3}{9}(\tilde{\rho} - 1)\frac{3(k_T R)^2 + 9ik_T R - 9}{(2\tilde{\rho} + 1)(k_T R)^2 + 9ik_T R - 9}, \tag{3}$$

where the mass density ratio appears as

$$\tilde{\rho} = \frac{\rho_p}{\rho}. \tag{4}$$

Generally speaking, resonances correspond to the poles of the scattering coefficients. If the matrix is assumed to be purely elastic, i.e., using for μ its zero-frequency, real value $\mu_0 = \rho(c_T^0)^2$, with $c_T^0 = 977$ m s $^{-1}$ the zero-frequency value of the transverse velocity, one of the poles of the denominator of Eq. (3) gives the following simple expression for the resonance frequency f_{res}:

$$f_{\text{res}} = \frac{3c_T\sqrt{8\tilde{\rho} - 5}}{4\pi R(2\tilde{\rho} + 1)} \tag{5}$$

and the quality factor Q of this resonance is given by

$$Q = \frac{1}{3}\sqrt{8\tilde{\rho} - 5}. \tag{6}$$

Using these approximate expressions, one finds $f_{\text{res}} = 425$ kHz and $Q = 3.4$ (respectively, $f_{\text{res}} = 337$ kHz and $Q = 3.4$)

for 397 μm (respectively, 500 μm) diameter beads in epoxy matrix. These approximate values of the resonance frequency differ from their exact values ($f_{res} = 465$ kHz for 397 μm diameter beads and $f_{res} = 366$ kHz for 500 μm diameter beads) by $<10\%$, which confirms the relevance of approximation (5). The approximate values of the quality factor are even closer to their exact values ($Q = 3.2$ for 397 μm diameter beads and $Q = 3.1$ for 500 μm diameter beads). It is also worth noting that, in this limit, Q only depends on the density contrast and is a monotonously increasing function of $\tilde{\rho}$ from $\tilde{\rho} = 5/8$. The same conclusion has already been drawn concerning the resonance of core-shell particles through numerical investigations.[19,50]

Finally, we address the influence of the matrix viscoelasticity on the dipolar resonance frequency. Viscoelasticity is indeed expected to play a noticeable role in the present case since the resonance frequency is close to the inverse of the first relaxation time τ_1. The actual resonance frequency can be numerically evaluated by solving Eq. (5) recursively: at the first iteration, the low frequency value of the matrix shear modulus is used for determining the resonance frequency $f_{res,1}$; at the second iteration, the value of the matrix shear modulus at frequency $f_{res,1}$ is used for determining the resonance frequency $f_{res,2}$, etc. One ultimately finds $f_{res} = 483$ kHz (respectively, $f_{res} = 381$ kHz) for 397 μm (respectively, 500 μm) diameter particles in epoxy. Viscoelasticity induces a relative frequency shift on the order of 4%.

B. Analogy with Minnaert resonance in bubbly liquids

In the $\tilde{\rho} \gg 1$ limit, f_{res} has the following approximate expression:

$$f_{res} \simeq \frac{3\sqrt{2}}{4\pi}\frac{1}{R}\sqrt{\frac{\mu}{\rho_p}}. \tag{7}$$

This resonance frequency f_{res} depends on the shear modulus *of the matrix*, i.e., of the most deformable under shear material, and on the inertia *of the particle*, i.e., of the densest material. This hybrid combination of mechanical properties in the factors determining this dipolar resonance is very similar to the Minnaert resonance of the volume oscillations (monopolar resonance) of a gas bubble in a liquid, for which the relevant stiffness is the one of the most compressible material (the gas) and the relevant inertia is the one of the densest material (the liquid). This is precisely the kind of hybridizationof mechanical properties of the two-components material which makes both the Minnaert resonance of bubbly liquids and the dipolar resonance of dense particles dispersed in an elastic matrix subwavelength.

C. Influence of the density contrast on resonance

Finally, we aim to numerically determine the influence of particle density and shear modulus on the propagation of the coherent wave. For simplicity purposes, the matrix is assumed to be purely elastic and has the epoxy density $\rho = 1100$ kg m ^{3} and the Lamé constants $\lambda = \lambda_0 = 3.6 \times 10^9$ Pa and $\mu = \mu_0 = 1.05 \times 10^9$ Pa. The beads diameter and volume fraction are fixed equal to 500 μm and $\phi = 2\%$. First, a numerical study is performed by varying the bead density ρ_p between 5500 kg m ^{3} and 22000 kg m ^{3} ($\tilde{\rho}$ ranging from 5 to 20) for fixed values of the bead Lamé constants $\lambda_p = 2.09 \times 10^{11}$ Pa and $\mu_p = 2.66 \times 10^{11}$ Pa, so that $\tilde{\mu} = 253$. The frequency dependences of the dimensionless velocity c_L^{eff}/c_L^0 and dimensionless attenuation $\alpha_L^{eff} R$ of the longitudinal coherent wave are plotted in Figs. 6(a) and 6(b), respectively, for four different values of $\tilde{\rho}$, together with the corresponding resonance frequencies f_i, $i = 1$ 4, computed using Eq. (5). First, we note that, as in the case of Minnaert resonance of bubbly liquids, the resonance frequency coincides with the inflection of attenuation and with the minimum of velocity. Moreover, the larger $\tilde{\rho}$ is, the larger are the variations of velocity and the attenuation at resonance, as expected from the predicted increase of the quality factor of the resonance with $\tilde{\rho}$. These observations complete the analytical study presented hereinabove.

D. Link between particle dynamics and effective acoustic properties

As analyzed in Refs. 36, 51, and 52, under the hypotheses of linear, Hookean elasticity Newton's principle applied to a single rigid particle moving in a viscoelastic matrix leads to the following differential equation that couples the particle displacement u_p and the matrix displacement u associated to the coherent wave at the particle location:

$$\frac{4}{3}\pi R^3 \rho_p \ddot{u}_p = 6\pi R\mu(u - u_p) + 6\pi R\mu\frac{R}{c_T}(\dot{u} - \dot{u}_p) + \frac{2}{3}\pi R^3\rho(\ddot{u} - \ddot{u}_p) + \frac{4}{3}\pi R^3\rho\ddot{u}. \tag{8}$$

Physical interpretation of the terms appearing in this differential equation is not present in the literature in the case of a solid matrix, contrary to the case of a fluid matrix. In this context, we compare the terms of the right-hand side (RHS) of Eq. (8) to those for the case of a viscous fluid matrix, i.e., Stokes viscous drag, Basset-Boussinesq history force, the added mass effect, and Archimedes force.[49] The first term of the RHS of Eq. (8) is an elastic spring force exerted by the matrix on the moving particle.[53,54] This spring force is associated to the matrix deformation which extends over a distance comparable to R and adapts to the particle displacement through the propagation of shear waves. The fourth term of the RHS can be interpreted as a time-dependent buoyancy (Archimedes-like force) associated to the matrix acceleration. In the low frequency $k_L R \ll 1$ regime considered here, adaptation of the matrix acceleration to the incident stress wave is instantaneous so that this time-dependent buoyancy is in phase with the matrix acceleration. On the contrary, since $c_T < c_L$, the spring force exerted by the matrix on the moving particle is expected to adapt to the particle displacement with a time delay on the order of R/c_T highlighting a relaxation process of the spring force over the characteristic timescale R/c_T. The third term of the RHS is the so-called added mass effect which has a noticeable influence on the resonance frequency although it has been neglected in Ref. 36. We note

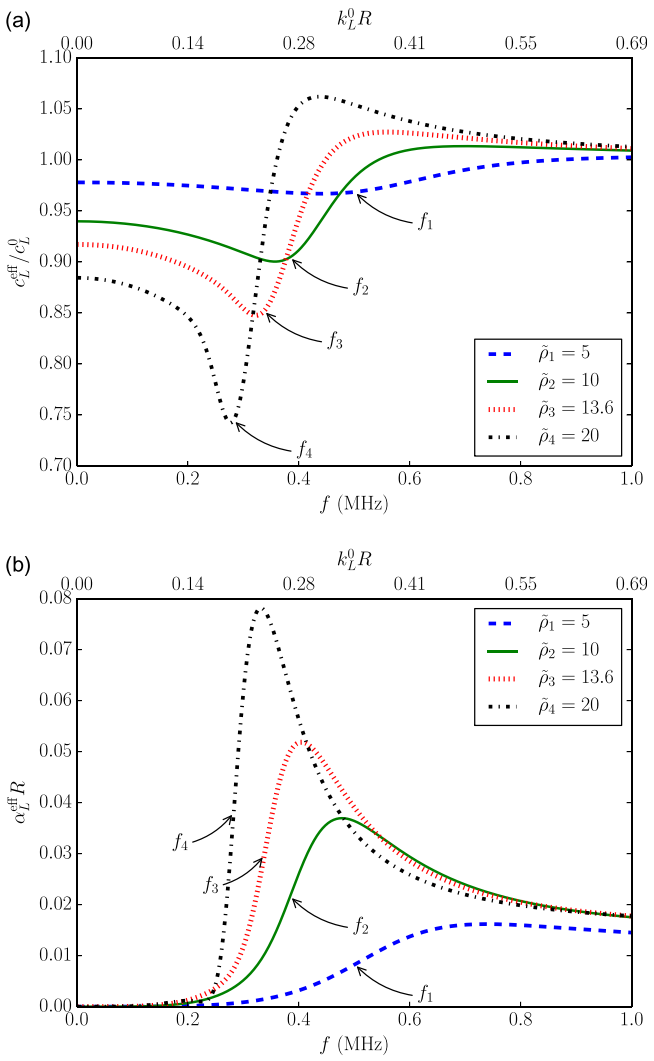

FIG. 6. (Color online) Variations of (a) dimensionless effective longitudinal velocity and (b) dimensionless effective longitudinal attenuation as function of frequency for various values of the mass density contrast ρ for a fixed value of the elasticity ratio μ 253. The resonance frequencies correspond ing to each value of ρ are also indicated.

that an additional source of time delay of the spring force originates from the viscoelastic properties of the matrix. Thus, the damping of the particle motion has two origins: the delay of propagation through the matrix close to the particle of shear stresses associated to its displacement, called hereafter elastic relaxation, which occurs without energy dissipation, and the viscoelastic nature of the matrix shear modulus μ, which involves energy dissipation, called hereafter viscoelastic relaxation. As shown in Ref. 55, damping of the particle motion due to elastic relaxation occurs through acoustic radiation.

The solution of Eq. (8) in the harmonic regime can be expressed as $u_p = t_p u$ where[49]

$$t_p = \frac{9(\tilde{\rho}-1)}{i(k_L R)^3} T_1^{LL}. \tag{9}$$

This expression evidences the link between the translational motion of the particle, the particle vibration mode $n=1$, and associated acoustic scattering.[49]

E. Influence of relaxation on effective acoustic properties

We now aim to analyze the impact of both elastic and viscoelastic relaxations on the dispersion equation and on effective acoustic properties of the dispersion. For simplicity purpose, we adopt Foldy's approximation for the dispersion equation, i.e., we consider Eq. (2) without the second-order term in concentration. In the low frequency regime $|k_L R| \ll 1$ considered here, the multipolar expansion in Eq. (2) can be safely restricted to the two first vibration eigenmodes ($n=0$ and $n=1$). The simplified dispersion equation we now consider is thus

$$\left(\frac{k_L^{\text{eff}}}{k_L}\right)^2 = 1 - i\frac{3\phi}{(k_L R)^3}\left(T_0^{LL} + 3T_1^{LL}\right), \tag{10}$$

where $T_0^{LL} = -i(k_L R)^3/3$ for a rigid particle.[49]

In both the numerator and denominator of Eq. (3), the imaginary number $9ik_T R$ represents the contribution of elastic relaxation on the phase shift of u_p with respect to u. Neglecting both elastic and viscoelastic relaxations, i.e., dropping $9ik_T R$ in Eq. (3) and using for μ its zero-frequency, real value μ_0, leads to the following expression for the effective wavenumber

$$\left(\frac{k_L^{\text{eff}}}{k_L}\right)^2 = 1 - \phi + \frac{\phi(\tilde{\rho}-1)[(k_T R)^2 - 3]}{(2\tilde{\rho}+1)(k_T R)^2 - 9}. \tag{11}$$

Under these assumptions, $(k_L^{\text{eff}})^2$ is real. Thus, depending on its sign, k_L^{eff} is either real or pure imaginary, i.e., the coherent wave is either progressive or evanescent. Analysis of Eq. (11) leads to identify a stop band, i.e., a frequency range for which evanescence occurs ($\text{Re}[k_L^{\text{eff}}] = 0$, $\text{Im}[k_L^{\text{eff}}] \neq 0$). The lower boundary of the stop band is the resonance frequency $f_{\text{res}}^0 = 3c_T/2\pi R\sqrt{2\tilde{\rho}+1}$, which differs from f_{res} as given by Eq. (5) as a consequence of the further simplifications applied to the propagation model. Its upper frequency is a cutoff frequency which has the following expression:

$$f_c = f_{\text{res}}^0 \sqrt{1 + \frac{2\phi(\tilde{\rho}-1)^2}{\phi(\tilde{\rho}-4) + 2\tilde{\rho}+1}}. \tag{12}$$

Note that such an expression for the upper boundary of stop band has been previously derived by Moon and Mow[36] and has been found to fit experimental measurements on dispersions of lead spheres in epoxy resin.[35]

This stop band is visible in Figs. 7(a) and 7(b), which display, respectively, the variations of the real and imaginary parts of k_L^{eff} as defined by Eq. (11) for the TC-epoxy dispersion as function of frequency for several values of ϕ. We now compare in Figs. 7(a) and 7(b) the frequency variations of k_L^{eff} without relaxation, i.e., as given by Eq. (11), to the ones of k_L^{eff} with elastic relaxation and with or without viscoelastic relaxation, i.e., as given by Eq. (10). The values chosen for the mechanical properties of the materials are those of TC-epoxy dispersion. Strikingly, elastic relaxation results in a considerable smoothing of the variations of $\text{Re}[k_L^{\text{eff}}]$ and

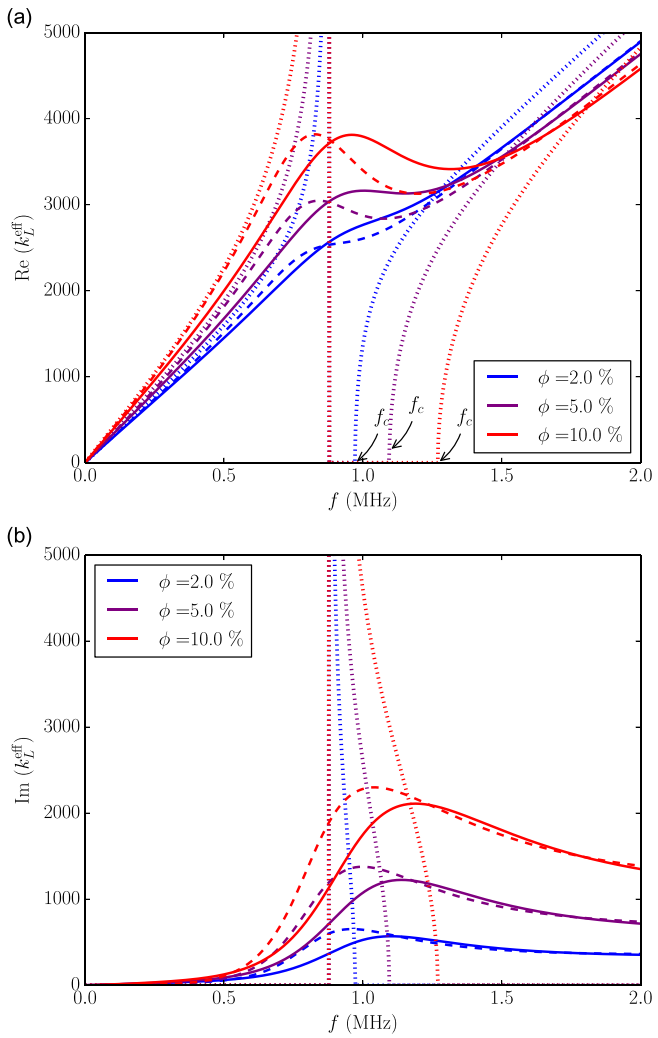

FIG. 7. (Color online) Variations of (a) the real part and (b) the imaginary part of the effective wavenumber as functions of frequency for several values of the beads volume fraction ϕ. Dotted curve, without elastic nor viscoelastic relaxation; solid curve, with elastic and viscoelastic relaxation; dashed curve, with elastic relaxation, without viscoelastic relaxation. The upper frequency of the stop band f_c is indicated in (a) for each value of ϕ.

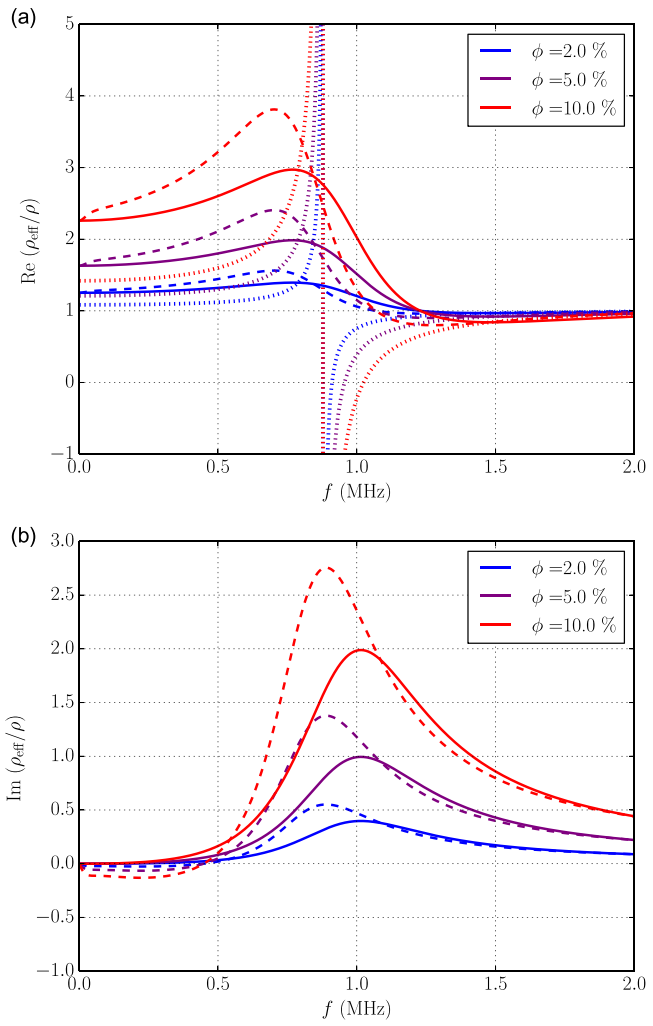

FIG. 8. (Color online) Variations of (a) the real part and (b) the imaginary part of the dimensionless effective mass density as functions of frequency for several values of the beads volume fraction ϕ. Dotted curve, without elastic nor viscoelastic relaxation; dashed curve, with elastic relaxation, without viscoelastic relaxation; solid curve, with elastic and viscoelastic relaxation.

$\text{Im}[k_L^{\text{eff}}]$. In particular, the stop band disappears, i.e., $\text{Re}[k_L^{\text{eff}}]$ is positive for all frequencies. Adding viscoelastic relaxation only slightly increases the frequency at which $\text{Re}[k_L^{\text{eff}}]$ is maximum and slightly decreases the maximum value of $\text{Im}[k_L^{\text{eff}}]$ compared to the case with elastic relaxation only. We conclude that *the main cause of smoothing of the dipolar resonance of the TC-epoxy dispersions studied here is elastic relaxation and not viscoelastic dissipation.*

Finally, we address the question of the impact of relaxation on effective mass density, which is expected to be affected by the dipolar resonance of the scatterers and is of particular interest in the context of acoustic metamaterials. In the frame of Foldy's model, the effective mass density of the dispersion ρ_{eff} is defined as[56]

$$\frac{\rho_{\text{eff}}}{\rho} = 1 - \frac{3i\phi}{2(k_L R)^3}\sum_{n=0}^{\infty}(2n+1)\left[1-(-1)^n\right]T_n^{LL}. \qquad (13)$$

In the low frequency regime $|k_L R| \ll 1$ considered here, the multipolar expansion in Eq. (13) can, here, also be safely restricted to the two first vibration eigenmodes, which results in the following approximate expression for ρ_{eff}:

$$\frac{\rho_{\text{eff}}}{\rho} \approx 1 - \frac{9i\phi}{(k_L R)^3}T_1^{LL}, \qquad (14)$$

and using Eq. (10), it yields

$$\frac{\rho_{\text{eff}}}{\rho} \simeq \phi + \left(\frac{k_L^{\text{eff}}}{k_L}\right)^2. \qquad (15)$$

Consequently, in the case of a steep resonance, we expect the stop band to approximately coincide with a frequency band of negative effective mass density. The real and imaginary parts of ρ_{eff} are plotted as functions of frequency, respectively, in Figs. 8(a) and 8(b) for several values of ϕ and for three cases: (i) absence of relaxation, (ii) elastic relaxation only, (iii) elastic and viscoelastic relaxation. The values chosen for the mechanical properties of the materials are, here, also those of TC-epoxy dispersion. As expected, in

absence of relaxation, ρ_{eff} is purely real and actually displays a frequency band of negative effective mass density. Taking into account elastic relaxation considerably smooths the variations of ρ_{eff}. In particular, the frequency band of negative mass density disappears, i.e., $\text{Re}[\rho_{\text{eff}}]$ is positive for all frequencies. Adding viscoelastic relaxation only slightly increases the frequency at which $\text{Re}[\rho_{\text{eff}}]$ and $\text{Im}[\rho_{\text{eff}}]$ are maximum and slightly decreases the maximum values of $\text{Re}[\rho_{\text{eff}}]$ and $\text{Im}[\rho_{\text{eff}}]$ compared to the case with elastic relaxation only. We conclude that the main cause of smoothing of the resonant behavior of the effective mass density of the TC-epoxy dispersion studied here is elastic relaxation.

Given these conclusions, the key phenomenon to be minimized for emphasizing the dipolar resonance is thus elastic relaxation around the resonance frequency, i.e., $k_T R$ has to be minimized at $f \sim f_{\text{res}}$. Given Eq. (5), $k_T R = [3\sqrt{8\tilde{\rho}} - 5]/[2(2\tilde{\rho} + 1)]$ at $f = f_{\text{res}}$, i.e., *at resonance*, $k_T R$ *depends only on* $\tilde{\rho}$ *and not on* $\tilde{\mu}$. This is in agreement with the independence versus $\tilde{\mu}$ of the quality factor of the resonance as given by Eq. (6). Thus, the larger the mass density contrast between the particle and the matrix, the steeper is the dipolar resonance.

We nevertheless recall that these conclusions have been drawn using Foldy's model. An open question is whether these conclusions hold in the frame of LCN model, which has been shown to precisely fit experimental data because it takes wave conversions into account. We note that there is presently no realistic model expressing the effective mass density in the case of an elastic matrix. Thus, investigation of the behavior of the effective mass density of such dispersions in which wave conversion noticeably affects acoustic propagation requires further theoretical developments.

V. CONCLUSION

Our experimental study of the acoustic transmission through random dispersions of rigid spheres in an elastic matrix in the vicinity of their subwavelength dipolar resonance, and its comparison with a recent model of effective propagation that fully accounts for the elastic nature of the matrix,[42] have allowed us to unambiguously demonstrate that wave conversion has a noticeable influence on the propagation of coherent longitudinal waves through such composite materials. Analyzing the dynamics of the scatterers has allowed us to evidence that the main cause of smoothing of the dipolar resonance is elastic relaxation, i.e., the finite time required for the shear stresses associated to the translational motion of the scatterers to propagate through the matrix. According to Foldy's multiple scattering model, we have shown that the only parameter that determines the dipolar resonance steepness is the particle to matrix mass density ratio. We have also shown that the effective mass density is affected by elastic relaxation in the same way as the dipolar resonance. This leads us to refine the benchmarking of rigid particles in an elastic matrix against dense core-soft shell particles regarding their ability to display negative effective mass density. We note that a possible asset of core-shell particles is a lesser impact of elastic relaxation on their dipolar resonance as the consequence of the confinement of elastic deformations in the thin shell. The phase delay associated to the propagation of shear stresses over the shell thickness e, $k_T e$ is indeed expected to be less than $k_T R$ provided that $e < R$. But at the same time, the confinement of elastic deformations in the thin shell is expected to lead to larger viscoelastic dissipation as compared to rigid particles in an elastic matrix, where deformations extend over a distance on the order of R. Thus, relaxation has an equivocal influence on the performances of both composite materials. This causes rather easy-to-make dispersions of rigid spheres in an elastic matrix appealing candidates as metamaterials.

ACKNOWLEDGMENTS

This work has been funded by Agence Nationale de la Recherche under Grant Metakoustik 2011-BS0902101, by Bordeaux University and by Centre national de la recherche scientifique (CNRS-Solvay) fund. The authors thank Lionel Bos, Thomas Brunet, and Valentin Leroy for fruitful discussions and helpful advice, and Isabelle Cantat and Jacques Marchal for technical support.

[1] Z. Liu, C. T. Chan, P. Sheng, A. L. Goertzen, and J. H. Page, "Elastic wave scattering by periodic structures of spherical objects: Theory and experiment," Phys. Rev. B **62**, 2446 2457 (2000).
[2] N. Fang, D. Xi, J. Xu, M. Ambati, W. Srituravanich, C. Sun, and X. Zhang, "Ultrasonic metamaterials with negative modulus," Nature Mater. **5**(6), 452 456 (2006).
[3] S. Zhang, L. Yin, and N. Fang, "Focusing ultrasound with an acoustic metamaterial network," Phys. Rev. Lett. **102**(19), 194301 (2009).
[4] C. Ding, L. Hao, and X. Zhao, "Two dimensional acoustic metamaterial with negative modulus," J. Appl. Phys. **108**(7), 074911 (2010).
[5] V. Leroy, A. Bretagne, M. Fink, H. Willaime, P. Tabeling, and A. Tourin, "Design and characterization of bubble phononic crystals," Appl. Phys. Lett. **95**(17), 171904 (2009).
[6] K. M. Ho, C. K. Cheng, Z. Yang, X. X. Zhang, and P. Sheng, "Broadband locally resonant sonic shields," Appl. Phys. Lett. **83**(26), 5566 5568 (2003).
[7] C. M. Park, J. J. Park, S. H. Lee, Y. M. Seo, C. K. Kim, and S. H. Lee, "Amplification of acoustic evanescent waves using metamaterial slabs," Phys. Rev. Lett. **107**(19), 194301 (2011).
[8] J. Pierre, B. Dollet, and V. Leroy, "Resonant acoustic propagation and negative density in liquid foams," Phys. Rev. Lett. **112**, 148307 (2014).
[9] S. Yao, X. Zhou, and G. Hu, "Experimental study on negative effective mass in a 1D mass spring system," New J. Phys. **10**(4), 043020 (2008).
[10] T. Brunet, A. Merlin, B. Mascaro, K. Zimny, J. Leng, O. Poncelet, C. Aristegui, and O. Mondain Monval, "Soft 3D acoustic metamaterial with negative index," Nature Mater. **14**, 384 388 (2014).
[11] L. Fok and X. Zhang, "Negative acoustic index metamaterial," Phys. Rev. B **83**, 214304 (2011).
[12] H. Chen, S. Zhai, C. Ding, S. Liu, C. Luo, and X. Zhao, "Meta atom cluster acoustic metamaterial with broadband negative effective mass density," J. Appl. Phys. **115**(5), 054905 (2014).
[13] S. H. Lee, C. M. Park, Y. M. Seo, Z. G. Wang, and C. K. Kim, "Composite acoustic medium with simultaneously negative density and modulus," Phys. Rev. Lett. **104**(5), 054301 (2010).
[14] M. Yang, G. Ma, Z. Yang, and P. Sheng, "Coupled membranes with doubly negative mass density and bulk modulus," Phys. Rev. Lett. **110**, 134301 (2013).
[15] K. Zimny, A. Merlin, A. Ba, C. Aristegui, T. Brunet, and O. Mondain Monval, "Soft porous silicone rubbers as key elements for the realization of acoustic metamaterials," Langmuir **31**(10), 3215 3221 (2015).
[16] T. Still, M. Oudich, G. K. Auerhammer, D. Vlassopoulos, B. Djafari Rouhani, G. Fytas, and P. Sheng, "Soft silicone rubber in phononic structures: Correct elastic moduli," Phys. Rev. B **88**, 094102 (2013).
[17] Z. Liu, C. T. Chan, and P. Sheng, "Analytic model of phononic crystals with local resonances," Phys. Rev. B **71**(1), 014103 (2005).
[18] M. Hirsekorn, "Small size sonic crystals with strong attenuation bands in the audible frequency range," Appl. Phys. Lett. **84**(17), 3364 3366 (2004).

[19]L. Bos, L. Lukyanova, and R. Wunenburger, "Constraints on the design of core shell resonators of locally resonant acoustic metamaterials," Phys. Rev. B **86**(18), 184107 (2012).
[20]V. K. Kinra, E. Ker, and S. K. Datta, "Influence of particle resonance on wave propagation in a random particulate composite," Mech. Res. Commun. **9**(2), 109 114 (1982).
[21]V. K. Kinra and V. Dayal, "A new technique for ultrasonic nondestructive evaluation of thin specimens," Exp. Mech. **28**(3), 288 297 (1988).
[22]L. W. Anson and R. C. Chivers, "Ultrasonic velocity in suspensions of sol ids in solids A comparison of theory and experiment," J. Phys. D **26**(10), 1566 1575 (1993).
[23]J. Wu, "Determination of velocity and attenuation of shear waves using ul trasonic spectroscopy," J. Acoust. Soc. Am. **99**(5), 2871 2875 (1996).
[24]R. E. Challis, F. Blarel, M. E. Unwin, J. Paul, and X. Guo, "Models of ul trasonic wave propagation in epoxy materials," IEEE Trans. Ultrason. Ferr. **56**(6), 1225 1237 (2009).
[25]R. E. Challis, F. Blarel, M. E. Unwin, and X. Guo, "On the modelling of ultrasonic bulk wave propagation in epoxies," J. Phys. Conf. Ser. **269**(1), 012001 (2011).
[26]R. M. Christensen, *Theory of Viscoelasticity* (Dover, New York, 1982), pp. 21 25.
[27]S. Chandrasekhar, "Stochastic problems in physics and astronomy," Rev. Mod. Phys. **15**(1), 1 89 (1943).
[28]B. Zeqiri, W. Scholl, and S. Robinson, "Measurement and testing of the acoustic properties of materials: A review," Metrologia **47**(2), S156 S171 (2010).
[29]H. Seki, A. Granato, and R. Truell, "Diffraction effects in the ultrasonic field of a piston source and their importance in the accurate measurement of attenuation," J. Acoust. Soc. Am. **28**(2), 230 238 (1956).
[30]M. B. Gitis and A. S. Khimunin, "Diffraction effects in ultrasonic mea surement (review)," Sov. Phys. Acoust. **14**(4), 413 431 (1969).
[31]This is equivalent to shifting in time S_a so as to bring the instant of detec tion t_p^1 (respectively, t_p^0) of the main peak of S_a (respectively, S_0) to zero.
[32]L. E. Kinsler, A. R. Frey, A. B. Coppens, and J. V. Sanders, *Fundamentals of Acoustics*, 3rd ed. (Wiley, New York, 1982), pp. 121 122.
[33]J. C. Bamber, "Attenuation and absorption," in *Physical Principles of Medical Ultrasonics*, edited by R. Hill, J. C. Bamber, and G. Haar (Wiley, New York, 2004), pp. 93 166.
[34]H. Wang, W. Jiang, and W. Cao, "Characterization of lead zirconate tita nate piezoceramic using high frequency ultrasonic spectroscopy," J. Appl. Phys. **85**(12), 8083 8091 (1999).
[35]V. K. Kinra and P. Li, "Resonant scattering of elastic waves by a random distribution of inclusions," Int. J. Solids Struct. **22**(1), 1 11 (1986).
[36]F. C. Moon and C. C. Mow, *Wave Propagation in a Composite Material Containing Dispersed Rigid Spherical Inclusions* (Research Memorandum Series, Rand Corporation, 1970), pp. 3 7.
[37]C. M. Linton and P. A. Martin, "Multiple scattering by random configura tions of circular cylinders: Second order corrections for the effective wavenumber," J. Acoust. Soc. Am. **117**(6), 3413 3423 (2005).
[38]J. Y. Kim, "Models for wave propagation in two dimensional random composites: A comparative study," J. Acoust. Soc. Am. **127**(4), 2201 2209 (2010).
[39]A. N. Norris and J. M. Conoir, "Multiple scattering by cylinders immersed in fluid: High order approximations for the effective wavenumbers," J. Acoust. Soc. Am. **129**(1), 104 113 (2011).
[40]S. K. Kanaun and V. M. Levin, "Propagation of longitudinal elastic waves in composites with a random set of spherical inclusions (effective field approach)," Arch. Appl. Mech. **77**(9), 627 651 (2007).
[41]J. M. Conoir and A. N. Norris, "Effective wavenumbers and reflection coefficients for an elastic medium containing random configurations of cy lindrical scatterers," Wave Motion **47**(3), 183 197 (2010).
[42]F. Luppé, J. M. Conoir, and A. N. Norris, "Effective wave numbers for thermo viscoelastic media containing random configurations of spherical scatterers," J. Acoust. Soc. Am. **131**(2), 1113 1120 (2012).
[43]J. G. Fikioris and P. C. Waterman, "Multiple scattering of waves. II. Hole corrections in the scalar case," J. Math. Phys. **5**, 1413 1420 (1964).
[44]M. Chekroun, L. Le Marrec, B. Lombard, and J. Piraux, "Time domain numerical simulations of multiple scattering to extract elastic effective wavenumbers," Waves Random Complex **22**(3), 398 422 (2012).
[45]M. Caleap, B. W. Drinkwater, and P. D. Wilcox, "Coherent acoustic wave propagation in media with pair correlated spheres," J. Acoust. Soc. Am. **131**(3), 2036 2047 (2012).
[46]R. E. Challis, M. J. W. Povey, M. L. Mather, and A. K. Holmes, "Ultrasound techniques for characterizing colloidal dispersions," Rep. Prog. Phys. **68**(7), 1541 1637 (2005).
[47]C. F. Ying and R. Truell, "Scattering of a plane longitudinal wave by a spherical obstacle in an isotropically elastic solid," J. Appl. Phys. **27**(9), 1086 1097 (1956).
[48]Y. H. Pao and C. C. Mow, "Scattering of plane compressional waves by a spherical obstacle," J. Appl. Phys. **34**(3), 493 499 (1963).
[49]T. Valier Brasier, J. M. Conoir, F. Coulouvrat, and J. L. Thomas, "Sound propagation in dilute suspensions of spheres: Analytical comparison between coupled phase model and multiple scattering theory," J. Acoust. Soc. Am. **138**(4), 2598 2612 (2015).
[50]A. O. Krushynska, V. G. Kouznetsova, and M. G. D. Geers, "Towards optimal design of locally resonant acoustic metamaterials," J. Mech. Phys. Solids **71**, 179 196 (2014).
[51]S. R. Aglyamov, A. B. Karpiouk, Y. A. Ilinskii, E. A. Zabolotskaya, and S. Y. Emelianov, "Motion of a solid sphere in a viscoelastic medium in response to applied acoustic radiation force: Theoretical analysis and ex perimental verification," J. Acoust. Soc. Am. **122**(4), 1927 1936 (2007).
[52]Y. A. Ilinskii, G. D. Meegan, E. A. Zabolotskaya, and S. Y. Emelianov, "Gas bubble and solid sphere motion in elastic media in response to acous tic radiation force," J. Acoust. Soc. Am. **117**(4), 2338 2346 (2005).
[53]A. Norris, "Faxén relations in solids A generalized approach to particle motion in elasticity and viscoelasticity," J. Acoust. Soc. Am. **123**(1), 99 108 (2008).
[54]A. Norris, "Impedance of a sphere oscillating in an elastic medium with and without slip," J. Acoust. Soc. Am. **119**(4), 2062 2066 (2006).
[55]H. L. Oestreicher, "Field and impedance of an oscillating sphere in a viscoelastic medium with an application to biophysics," J. Acoust. Soc. Am. **23**(6), 707 714 (1951).
[56]C. Aristegui and Y. C. Angel, "Effective mass density and stiffness derived from P wave multiple scattering," Wave Motion **44**(3), 153 164 (2007).